



Application of polyurethane foam/zinc oxide nanocomposite for antibacterial activity, detection, and removal of basic dyes from wastewater

E. A. Moawed¹ · M. S. Eissa¹ · S. A. Al-Tantawy¹

Received: 25 May 2020 / Revised: 5 April 2022 / Accepted: 11 July 2022 / Published online: 30 July 2022
© The Author(s) 2022

Abstract

In this paper, a new multifunctional nanocomposite was synthesized to combine both the advantages of sorption properties and antibacterial efficiency. The thiourea polyurethane/zinc oxide nanocomposite was prepared by coupling thiourea polyurethane foam and zinc oxide nanoparticles. The thiourea polyurethane/zinc oxide was characterized using several tools. The change in the surface chemistry of the thiourea polyurethane/zinc oxide nanocomposite (surface area was increased from 2.8 to 10.6 m²/g), due to the attached functional groups, increased its sorption properties. Also, the thiourea polyurethane/zinc oxide showed a crystalline phase, embedded inside the amorphous structure, with good thermal stability to 230 °C. The pore volume and radius of thiourea polyurethane/zinc oxide were 0.017 cm³/g and 3.4 nm with mesopores/micropores ratio of 11:1. It combines collecting pollutants on its surface, the ability to degrade these pollutants, and a good antibacterial effect. Thiourea polyurethane/zinc oxide was applied for the removing toluidine blue and brilliant green basic dyes from the wastewater. Several parameters such as pH, dye concentration, temperature, and time were studied. The removal percentages of brilliant green and toluidine blue dyes from the wastewater were 92.4–98.2% at pH 3–12. Also, the removing rate of the dyes was very fast (3–5 min) at 25 °C. The estimated capacities of new nanocomposite for toluidine blue and brilliant green were 92 and 227 mg/g. The removal process was spontaneous (ΔG was -7.3 and -8.6). As a result, the applicability of thiourea polyurethane/zinc oxide as an effective renewable antibacterial sorbent for removing cationic dyes was maintained.

Keywords Antibacterial efficiency · Cationic dyes · Nanocomposite · Polyurethane · Wastewater

Introduction

Water pollution has become one of the most important research subjects in recent years. Water is an essential and general need of human life and organisms due to its importance for drinking, agriculture, and daily activities. If the water becomes contaminated due to pollution, it can be harmful to humans and wildlife (Kiwaan et al. 2020; Jiang et al. 2020). Major of these pollutants are the organic dyes which used in veterinary medicine, textile, and plastic industries (Maleki et al. 2017; Hicham et al. 2019; Mohanraj et al. 2020). The wastewater contaminated with cationic dyes such

as brilliant green and toluidine blue can cause cancer of the bladder and retinal liver sarcoma (Moawed et al. 2019a, b, c; Islam et al. 2019). Many studies are looking for ways to remove dyes from the wastewater. Adsorption is the adhesion of contaminated particles on the surface of solid molecules, and it is the most preferable technique for wastewater treatments (Zhang et al. 2019; Hou et al. 2020). While the photodegradation technique destroys the dyes and other organic species in wastewater, therefore it is used intentionally in some disinfection technologies (Li et al. 2019; Yilmaz et al. 2020).

Polyurethane foam (PUF) has been widely used as a good sorption material due to its efficiency, low cost, easy handling, and storage. The presence of polar and nonpolar functional groups in PUF makes it more proper to sorbate different materials (Moawed et al. 2019a, b, c). Besides, polyurethane foam can be recycled easily after the desorption of pollutants. The high basicity of PUF decreases the sorption capacity of basic dyes and metal ions (Moawed

Editorial responsibility: Samareh Mirkia.

✉ E. A. Moawed
eamoawed@yahoo.com

¹ Chemistry Department, Faculty of Science, Damietta University, P.O. Box: 34517, New Damietta, Egypt



and El-Shahat 2013). Therefore, many reports studied the uses of the PUF with coupling with ligand through an azo group (Moawed and El-Shahat 2006), grafting with chelating reagent (El-Shahat et al. 2007), the substitution of its functional groups (Moawed et al. 2017), or immobilization with specific reagents (Stenholm et al. 2020). In this paper, the thiourea polyurethane/zinc oxide nanocomposite was prepared by replacing the basic functional groups (primary amines) of PUF with thiourea groups; then, coupling with zinc oxide can increase its sorption properties.

Zinc oxide nanoparticles (ZnONP) have received more concerns over the last few years due to specific physical and chemical properties. Also, ZnONP exhibits thermal stability and attractive antibacterial properties (Cao et al. 2009; Mohamed et al. 2019). Moreover, ZnONPs are low cost and relatively nontoxic to the environment (Moawed et al. 2019a, b, c; Xu et al. 2019). Generally, the addition of ZnONP to sorbents not only improves its properties, whether adsorption or catalytic degradation of pollutants, but also enhances its antibacterial effect (Mostafa et al. 2020; Tang et al. 2020).

In this paper, TPUF/ZnO was synthesized to combine both the advantages of sorption properties of TPUF and the antibacterial efficiency of ZnONP. Polyurethane foam (PUF) was modified with thiourea groups. ZnONP was then refluxed with the thiourea polyurethane foam (TPUF) in ethanol. TPUF/ZnO was characterized using XRD, SEM, IR, UV–Vis, BET, and TGA. The activity of TPUF/ZnO was investigated for the detection and removal of brilliant green (BG) and toluidine blue (TBO) basic dyes from wastewater of Damietta industrial city, Egypt. The wastewater samples were collected from five places for a duration of 7 weeks. The effects of time, dye concentration, pH, and temperature were examined. Also, the antibacterial activity of TPUF/ZnO was tested against *Escherichia coli* (*E. coli*), *Staph aureus* (*S. aureus*), and *Salmonella* food poisoning bacteria.

Materials and Methods

Materials

We added the following sentences: Commercial PUF ($d = 12 \text{ kg/m}^3$) was supplied from Foamex Company for foam production, Damietta, Egypt. All chemicals used in the experiment were purchased from Sigma-Aldrich (USA) and Adwic (Egypt). Commercial PUF sheets were supplied by the Egyptian company for foam production.

Preparation of ZnONP

A 15 mL of NH_4OH (7 mol/L) solution was added to 150 mL of $\text{ZnSO}_4 \cdot 7\text{H}_2\text{O}$ solution (0.5 mol/L), and then, 15 mL of

NaHCO_3 solution (3 mol/L) was added drop by drop. A colloid of zinc hydroxy carbonate was formed at 60 °C (30 min), filtered, and washed with distilled water and ethanol. The colloid was dried at 110 °C overnight and calcined at 400 °C for 2 h to form ZnONP (Cao et al. 2007; Moawed et al. 2019a, b, c).

Preparation of TPUF

A 10 g of PUF cubes was soaked in 1 mol/L HCl overnight and then washed with distilled water. A 50 mL of concentrated HCl and then 25 mL of NH_4SCN solution (5 g/L) were added to PUF.

Preparation of TPUF/ZnO nanocomposite

A TPUF was refluxed with 2 g of ZnONP in 200 mL ethanol for 6 h. The TPUF/ZnO was washed with solutions of 0.1 mol/L HCl and 0.1 mol/L NaOH followed by ethanol and dried in air.

Preparation of dye solutions

A 0.1 g of toluidine blue ($\text{C}_{15}\text{H}_{16}\text{ClN}_3\text{S}$, 305.8 g/mol) and brilliant green ($\text{C}_{27}\text{H}_{34}\text{N}_2\text{O}_4\text{S}$, 482.6 g/mol) were dissolved in 100 mL distilled water.

Apparatus

XRD pattern of TPUF/ZnO was investigated using an X-ray diffractometer (D8-Brucker) equipped with Cu $\text{K}\alpha$ radiation ($\lambda = 1.54 \text{ \AA}$). The surface morphology of TPUF/ZnO was examined using SEM, JEOL) JSM-6510LV, USA (. The electrical conductivity of TPUF/ZnO was evaluated in the solid state using Keithley (6517B electrometer). FTIR spectrum was performed by JASCO-410 spectrometer (JASCO, Easton, MD). UV–Vis spectrophotometer (JASCO, V-630, Japan) was employed for absorbance measurements. The sorption/desorption isotherm of N_2 onto TPUF/ZnO composite at $-196 \text{ }^\circ\text{C}$ was evaluated using NOVA 3200, USA apparatus. Thermal analysis (TGA, DTA, and DSC) of TPUF/ZnO was estimated at 29–1000 °C by DSC-TGA device model (SDTQ 600, USA) under N_2 atmosphere (flow rate of 100 mL/min and a heating rate of 10 °C/min).

General procedures

TPUF/ZnO capacities (Q) and dye removal percentage ($\%E$) were estimated using batch technique at pH (1–14), time (3–60 min), and temperature (25–85 °C). A 25 mL of (100–1000 μg) brilliant green or toluidine blue solutions amounts of BG and TBO dyes were shaken with 100 mg of

TPUF/ZnO. The percentage of dye removal and sorption capacity were investigated using the following equations.

$$\%E = \frac{C_0 - C_e}{C_0} \times 100 \quad (1)$$

$$Q = C_0EV/m \quad (2)$$

where C_0 and C_e are the initial and remaining dye concentration (mg/L), V is the volume of toluidine blue and brilliant green, and m is the weight of TPUF/ZnO (g).

Results and discussion

Characterization of TPUF/ZnO

The surface morphology of TPUF/ZnO nanocomposite was investigated using SEM images with different magnifications (100–20,000x) as shown in Figs. 1 and S1. The SEM image at 500× magnification (Fig. 1A) illustrates that the surface of TPUF was coated with ZnONP. It also shows that

the ZnONP was adsorbed inside TPUF spaces. Higher magnification of TPUF/ZnO nanocomposite images, at 5000x, 10,000x, and 20,000x, shows that the crystals of ZnONP were aggregated onto the surface of TPUF. Also, it reveals that ZnONP was converted from a spherical shape (Moawed et al. 2019a, b, c) to a hexagonal shape in TPUF/ZnO (Fig. 1, S1). Therefore, SEM analyses confirmed the successful coupling between ZnONP and TPUF.

The XRD patterns of TPUF/ZnO nanocomposite showed strong and narrow diffraction peaks (Fig. 2), which refers to the good crystallinity of the TPUF/ZnO. A broad diffraction band was observed at 19.8°, which indicates the amorphous character of TPUF/ZnO. The intensity of this band was decreased from 84 to 37 counts, and it was shifted from 20.9 to 19.8° (Fig. 2, 2S). The formation of TPUF/ZnO composite with a significant change of the amorphous phase was indicated. The diffraction peaks of TPUF/ZnO at 31.9, 34.5, 36.4, 47.6, 56.8, 63.0, 68.3, and 76.9° were attributed to ZnONP. These diffraction peaks show the hexagonal wurtzite phases of ZnONP. Similar results were reported in the Joint Committee on Powder Diffraction Standards (JCPDS file PDF NO. 36-1451) (Shatnawi et al. 2016).

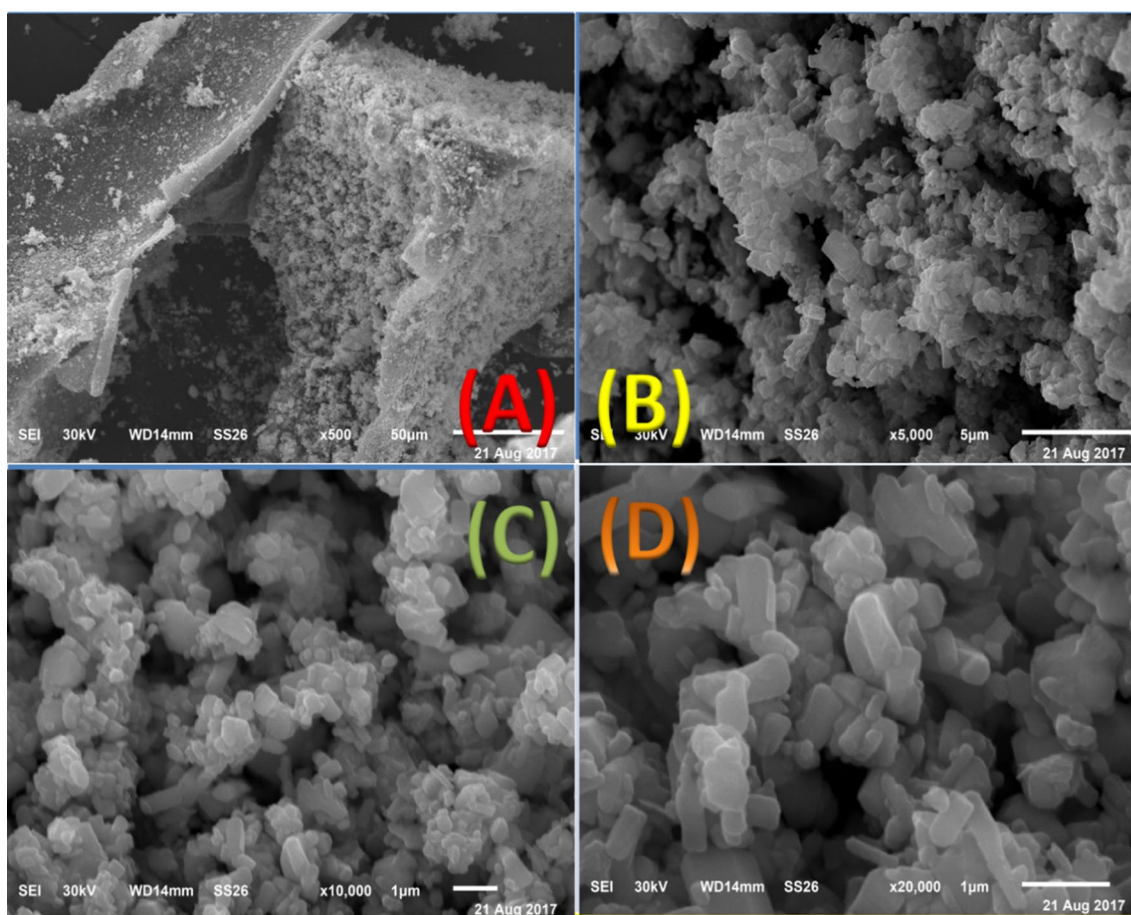


Fig. 1 Surface morphology of TPUF/ZnO

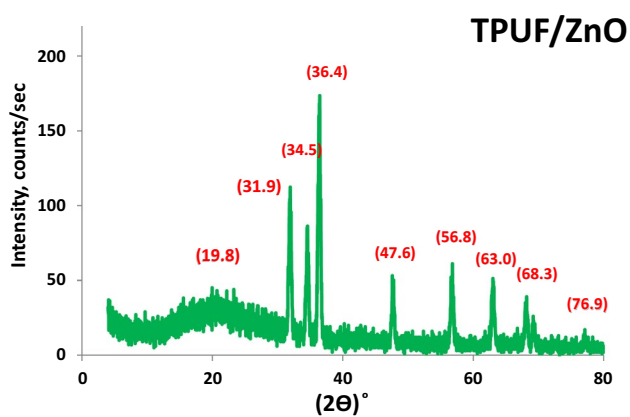


Fig. 2 XRD patterns of TPUF@ZnO

However, the diffraction peaks at 2θ around 41, 50, and 58° indicate the coupling between TPUF and ZnONP. The particle size (D) of TPUF/ZnO was calculated from the diffraction peaks using the Debye–Scherrer equation ($D = 0.89\lambda/\beta \cos \theta$) where λ is the wavelength of X-rays, θ is the Bragg diffraction angle, and β is the full width at half-maximum (FWHM) of the diffraction peak. The average particle size of TPUF/ZnO nanocomposite is 18.4 nm.

Surface area and pore volume of TPUF/ZnO were estimated using BET and BJH techniques. The N_2 adsorption/desorption isotherm of TPUF/ZnO was nearly similar to type-IV of IUPAC classification, which dominates the mesopores property (Fig. 3A). The isotherm showed that the adsorbed amount of N_2 was increased gradually with increases in the relative pressure. The hysteresis loop was exhibited H3 type, which generally corresponds to aggregates of platelike particles or slit-shaped pores. The BET

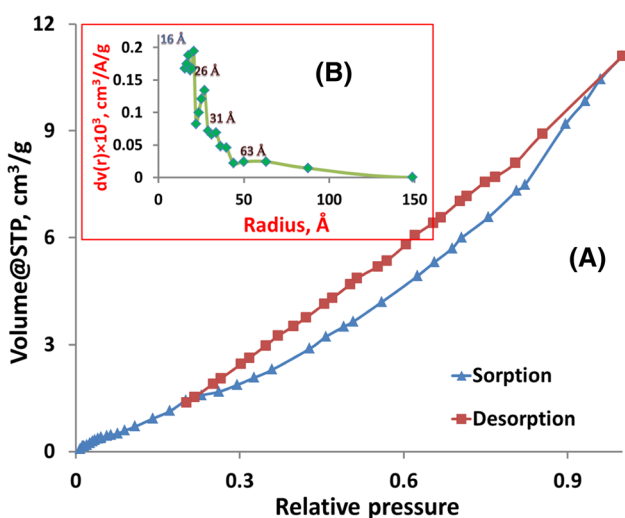


Fig. 3 BET and BJH curves for the sorption and desorption of N_2 gas onto TPUF@ZnO

surface area of TPUF/ZnO ($10.6 \text{ m}^2/\text{g}$) was higher than that of PUF ($2.8 \text{ m}^2/\text{g}$) and lower than that of ZnONP ($31.5 \text{ m}^2/\text{g}$). ZnONP was grafted within the TPUF matrix as shown in Fig. S3. Barrett/Joyner/Halenda (BJH) method was used to find pore volume and pore radius of TPUF/ZnO. The averages of pore radius and pore volume were found 34 \AA (3.4 nm) and $0.017 \text{ cm}^3/\text{g}$ for TPUF/ZnO (Fig. 3B). The mesopores/micropores volumes ratio ($1.7 \times 10^{-2} \text{ cm}^3/\text{g}$: $1.5 \times 10^{-3} \text{ cm}^3/\text{g}$) was 11:1.

FTIR spectroscopy was used for the characterization of specific TPUF/ZnO functional groups (Fig. 4). A broad-band appeared from 3421 to 3112 cm^{-1} was assigned to NH and OH groups ($\nu_{\text{NH/OH}}$). Several sharp peaks were also observed at 2910 , 2867 , 2857 cm^{-1} (ν_{CH}), 1668 cm^{-1} (ν_{CO}), 1639 cm^{-1} ($\nu_{\text{C=C}}$), and 1525 cm^{-1} (ν_{COC}), which characterize the matrix of PUF. The new characteristic peaks for N=C=S , N=C , and Zn-O , appeared at 2075 , 1540 , and 433 cm^{-1} , result from the coupling of TPUF matrix and ZnONP.

The optical bandgap of TPUF/ZnO was estimated according to the following equation [$ah\nu = B(h\nu - E_g)^m$] where E_g is the bandgap energy, a is the absorption coefficient, $h\nu$ is the incident photon energy, and B and m are constants. A plot of $(ah\nu)^{1/m}$ versus $h\nu$ gives the value of the bandgap, where $m=2$ for the indirect transition. The bandgap energy of TPUF/ZnO was estimated as 2.5 eV .

Electrical conductivity (σ) of TPUF/ZnO, PUF, and ZnO was 7.1×10^{-8} , 1.6×10^{-8} , and $6.1 \times 10^{-7} \Omega^{-1} \text{ m}^{-1}$. This increase in conductivity of TPUF/ZnO shows the relative improvement of the polarity of TPUF/ZnO due to the increases in the number of charge carriers (Zn-O).

TGA curve of TPUF/ZnO shows a smooth stepwise manner, containing five steps of thermal decomposition (Fig. 5A). The first decomposition of TPUF/ZnO begins at 229°C accompanied with weight loss of 1.6, 31.1, 44.6, 11.1, and 13.2% at temperature ranges of $227\text{--}229$, $230\text{--}312$, $313\text{--}421$, $421\text{--}824$, and $> 824^\circ \text{C}$, respectively. In the first steps, the weight loss of TPUF/ZnO comes

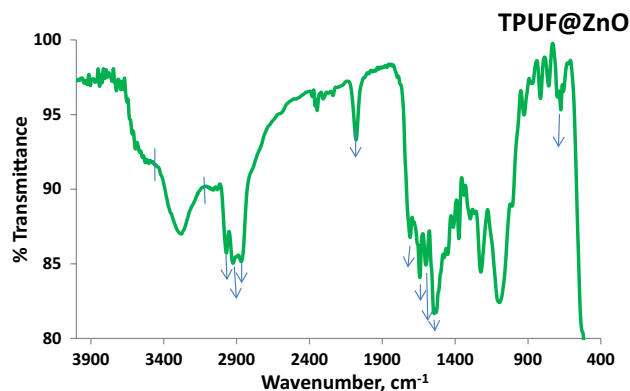


Fig. 4 Infrared spectra of TPUF@ZnO

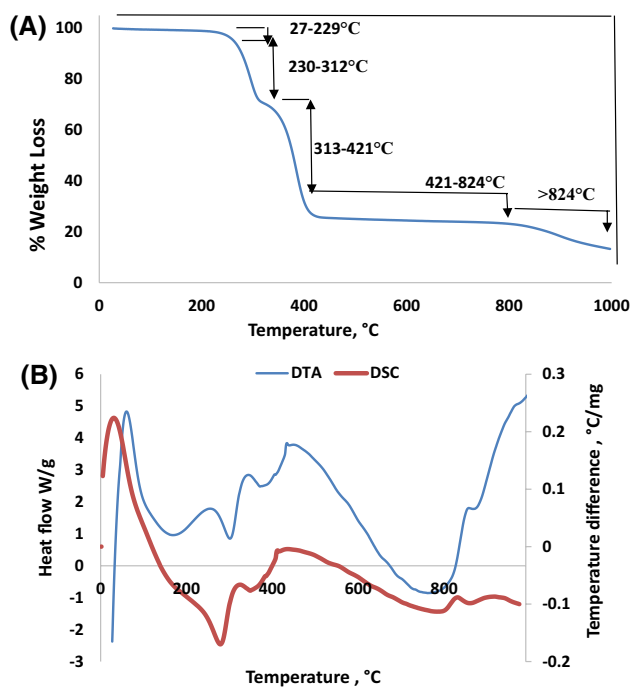


Fig. 5 TGA, DSC, and DTA curves of TPUF@ZnO nanocomposite

from the evaporation of adsorbed water molecules. The major weight losses (75.7%) occur at temperature ranged between 230 and 421 °C, due to the decomposition of TPUF matrix. The last decomposition occurs (11.1%) at 421–824 °C due to the crystallinity of ZnO. At $T > 421$ °C, the remaining weight loss of TPUF/ZnO (24.3 wt%) represents the percentage content of ZnONP in TPUF/ZnO.

DTA curve of TPUF/ZnO shows four endothermic peaks at 305, 377, 805, and 880 °C and two exothermic peaks at 62 and 943 °C (Fig. 5B). DTA curve of PUF shows two endothermic peaks at 288.5 and 356.8 °C while DTA curve for ZnO shows two exothermic peaks at 370 and 520 °C. Therefore, these results support the chemical interaction between TPUF and ZnO.

The chemical stability of TPUF/ZnO nanocomposite was tested in different buffer solutions (pH:1–14) and different organic solvents (e.g., CH₃OH, C₂H₅OH, CH₃COCH₃, C₆H₆, C₆H₅CH₃, DMF, and DMSO). 0.5 g of the TPUF/ZnO was soaked in 25 mL of each buffer solution and organic solvent for 24 h, then filtrated, dried, and weighted. The weights of TPUF/ZnO were not affected (Fig. S4), which confirms the good chemical stability of TPUF/ZnO in the presence of tested solutions and solvents.

The stability of TPUF/ZnO was also studied by reusing it. The sorption capacities of TPUF/ZnO for brilliant green and toluidine blue dyes were 0.47 and 0.30 mmol/g (Table 1). Regeneration of TPUF/ZnO nanocomposite was investigated by stripping dye molecules from TPUF/ZnO nanocomposite

Table 1 Characteristics of isotherms curve for the sorption of dyes onto TPUF@ZnO

Dye	Least square equation		R^2	LOD μg/L	Q mmol/g
	Slope	Intercept			
Brilliant green	0.012	0.013	0.962	2.5	0.47
Toluidine blue	0.018	0.019	0.990	2.9	0.30

using ethanol. The capacity of TPUF/ZnO was not affected after ten recycling of removals.

Application of TPUF/ZnO

Antibacterial activity

The antibacterial activity of TPUF/ZnO was tested against bacterial pathogen *Escherichia coli* (*E. coli*), *Staph aureus* (*S. aureus*), and *Salmonella typhimurium* (*S. Typhimurium*). A 0.05 g of TPUF/ZnO was added to a 5-mL tube of nutrient broth containing an overnight suspension of each bacterial culture. Measuring the optical density (OD) at 600 nm is a simple and widely used method to monitor the growth of microorganisms in liquid culture. The optical density (OD_{600nm}) was measured at 600 nm every 1 h, and the growth curve was performed. A decrease in bacterial growth on bacterial cultures containing TPUF/ZnO was observed while the bacterial growth of blank cultures (without TPUF/ZnO) was increased with the same increase in time (Fig. 6).

Detection of cationic dyes in water

The detection of brilliant green (BG) and toluidine blue (TBO) dyes in different samples of wastewater was examined under dark condition. The detection limits (LOD) and limits of quantitation (LOQ) are established using the equation (LOD = 3σ and LOQ = 10σ), where σ is the standard deviation for 5 replicating procedures. The values of LOD were 2.5 and 2.9 μg/L ($n=5$, Table 1) which indicate sensitive detection of dyes using TPUF/ZnO. Besides, the values of LOQ were 8.3 and 11.3 μg/L. The relative standard deviation values (RSD %) were 0.98 and 1.21 for 5 replicating procedures. Lower values of RSD% indicate the accuracy and precision of TPUF/ZnO for the detection of cationic dyes as a trace concentration.

The plot of the amount of dye per unit mass of TPUF/ZnO (capacity, Q) with concentrations of BG and TBO showed linear curves with good correlation coefficient (R^2) (0.962 and 0.990) and zero intercept (0.013 and 0.019) (Table 1). Also, the estimated capacity (Q) of TPUF/ZnO for brilliant green and toluidine blue was 0.47 and 0.30 mmol/g (227.0 and 91.7 mg/g). The result indicates that TPUF/ZnO has better sorption capacity than other sorbents (Table 2).



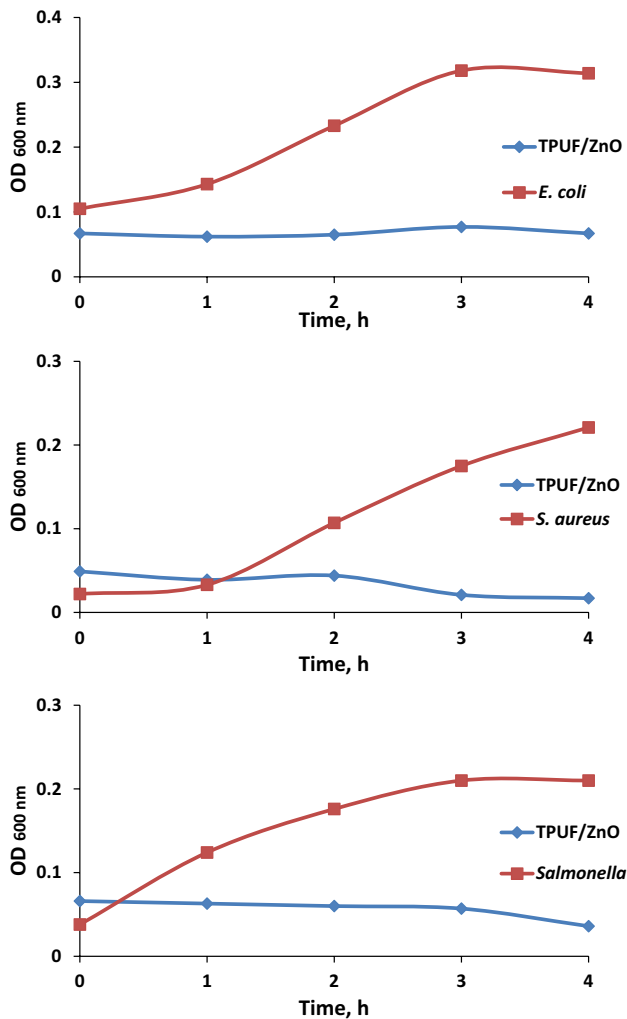


Fig. 6 Plot of optical density (OD_{600nm}) and the growth curve of *E. coli*, *S. aureus*, and *Salmonella* onto TPUF/ZnO

Removal of cationic dyes from wastewater

Wastewater samples were collected from a well in Damietta city. The water properties of wastewater are turbidity: 4.9, pH: 7.4, TDS: 280 mg/L, COD: 48 ppm, TOC: 6 ppm, total alkalinity: 140 mg/L, total hardness: 179 mg/L, Ca: 100 mg/L, Cl: 39 mg/L, SO₄: 65 mg/L, Fe 0.5 mg/L, and Mn 0.3 mg/L.

TPUF/ZnO was applied to remove brilliant green and toluidine blue dyes from industrial wastewater samples. The effects of pH (1–14), time (3–60 min.), and temperature (25–85 °C) on the removal of BG and TBO from aqueous solution were examined. The removal percentages of BG and TBO dyes were 95–100% at pH ranges 4–12 and 3–12 (Fig. S5).

The removals of BG and TBO were slightly affected by the pH changes (3–13). The little removal percentages at pH ≤ 1 are due to the repulsion between the cationic dyes and TPUF/ZnO particles (after surface protonation). These results show that it is unnecessary to adjust the pH of most industrial wastewater before the removal of BG and TBO.

The effect of time for removing of BG and TBO using TPUF/ZnO was investigated at different times. The time for maximum removal percentages of BG and TBO from wastewater was 3–5 min (Fig. S6). The removal percentages of BG and TBO dyes were slightly affected by increasing temperature. The negative values of ΔG° (−7.3 and −8.6 kJ/mol) for removal of BG and TBO dyes indicate spontaneous processes.

A 25 mL of industrial wastewater samples was spiked with different amounts of BG and TBO dyes (100–1000 µg); then, the solutions were shaken for 30 min with 0.1 g of TPUF/ZnO. The removal percentages of BG and TBO dyes from the industrial wastewater samples were found 96.8% and 95.5%. The relative standard deviations (RSD%) for 5 replicating procedures were 0.94 and 1.79%.

TPUF/ZnO nanocomposite was applied for the removal of BG and TBO dyes from different locations of water

Table 2 Comparison of maximum sorption capacities of various sorbents for dye removal

Sorbents	Dye	Q (mg/g)	References
Amine modified tannin gel	Brilliant green	20.4	Akter et al. (2016)
Turkish zeolite	Toluidine blue	64.0	Alpat et al. (2008)
NaOH-modified Walnut Shell	Brilliant green	123.2	Ashrafi et al. (2018)
MPGel	Brilliant green	150.0	De Castro Silva et al. (2018)
Iodopolyurethane powder	Brilliant green	154.4	Moawed, El-Shahat, (2016)
PUF@IT@MNPs	Brilliant green	224.8	Moawed et al. (2018)
Polyurethane@salvadora persica	Brilliant green	202.7	Moawed et al. (2018)
LGB/St/Al ₂ O ₃	Brilliant green		Moawed et al. (2018)
Gypsum _{Gypsum}	Toluidine blue	28.0	Rauf et al. (2009)
TPUF@ZnO	Brilliant green	227.0	This work
	Toluidine blue	91.7	



samples. Over thirty of Nile water, laundry water, and industrial wastewater samples from different places in industrial Damietta city for the duration of 1 year were collected. The average removal percentages of dyes from the Nile water, laundry water, and industrial wastewater samples were 97.3, 79.8, and 95.2%. The values of RSD% were 4.2, 2.5, and 1.8%, which considered as a relevant value (less than 10%) for water samples (Table 3).

Removal mechanism

The broadband of NH/OH in TPUF/ZnO was shifted to 3559–3170 and 3567–3139 cm^{-1} in spectra of TPUF/ZnO:BG and TPUF/ZnO:TBO (Fig. S7). Also, the band of N=C=S was shifted to 2086 and 2078 cm^{-1} ; besides, the Zn–O band was shifted to 420 and 416 cm^{-1} .

The plotting of Q versus $t^{1/2}$ (Weber–Morris model) gives a straight line that does not pass through the origin. The diffusion rates for the removal of BG and TBO (k_i) were 0.74 and 0.85 $\text{mg/g min}^{0.5}$ (Fig. S8). The lower molecular weight of TBO was the faster diffusion rate than BG, and k_i was dependent on the dye molecular weight.

The R^2 value for the removal of BG and TBO dyes proves that the removal process is fitted by pseudo-second-order model (0.9999 and 0.9993) rather than pseudo-first order (0.369 and 0.434, Fig. S9). The calculated rate constants (k_2) were 0.28 and 0.16 g/mg min , while the initial rate constants (h) were 2.99 and 2.09 min g/mg for the removal of BG and TBO. The rate for removal of BG was faster than that of TBO, and k_2 was independent on the dye molecular weight.

Conclusion

Our study was concerned with the preparation of TPUF/ZnO as a new multifunctional nanocomposite. The capability of TPUF/ZnO for the detection was 2.5 and 2.9 $\mu\text{g/L}$ BG and TBO dyes in the wastewater with removal percentages of 92.4–98.2%. The antibacterial effect of TPUF/ZnO against *Escherichia coli* (*E. coli*), *Staph aureus* (*S. aureus*), and *Salmonella* was also investigated and confirmed (a decrease in bacterial growth on bacterial cultures). The time required

for the complete removal of BG and TBO dyes from wastewater was 5 min at pH 3–9 and 25 °C. The capacities of TPUF/ZnO nanocomposite were 0.47 and 0.30 mmol/g for BG and TBO dyes. Kinetics of BG and TBO dye removals were described by pseudo-second-order model. The TPUF/ZnO nanocomposite was successfully applied for removing BG and TBO dyes from 5 replicating wastewater samples, with a relatively low standard deviation (0.98–1.21%) and low detection limit (2.5 and 2.9 $\mu\text{g/L}$).

Supplementary Information The online version contains supplementary material available at <https://doi.org/10.1007/s13762-022-04428-w>.

Acknowledgments The authors would like to appreciate the support of the Chemistry Department, Faculty of Science, Damietta University, Damietta, Egypt.

Funding Open access funding provided by The Science, Technology & Innovation Funding Authority (STDF) in cooperation with The Egyptian Knowledge Bank (EKB).

Declarations

Conflicts of interest The author declare that they have no conflicts of interests.

Open Access This article is licensed under a Creative Commons Attribution 4.0 International License, which permits use, sharing, adaptation, distribution and reproduction in any medium or format, as long as you give appropriate credit to the original author(s) and the source, provide a link to the Creative Commons licence, and indicate if changes were made. The images or other third party material in this article are included in the article's Creative Commons licence, unless indicated otherwise in a credit line to the material. If material is not included in the article's Creative Commons licence and your intended use is not permitted by statutory regulation or exceeds the permitted use, you will need to obtain permission directly from the copyright holder. To view a copy of this licence, visit <http://creativecommons.org/licenses/by/4.0/>.

References

- Akter N, Hossain MA, Hassan MJ, Amin MK, Elias M, Rahman MM, Asiri AM, Siddiquey IA, Hasnat MA (2016) Amine modified tannin gel for adsorptive removal of Brilliant Green dye. *J Environ Chem Eng* 4:1231–1241
- Alpat SK, Ozbayrak O, Alpat S, Akçay H (2008) The adsorption kinetics and removal of cationic dye, Toluidine Blue O, from aqueous solution with Turkish zeolite. *J Hazard Mater* 151:213–220
- Ashrafi M, Bagherian G, Chamjangali MA, Goudarzi N (2018) Removal of brilliant green and crystal violet from mono- and bi-component aqueous solutions using NaOH-modified walnut shell. *Anal Bioanal Chem Res* 5:95–114
- Cao Z, Zhang Z, Wang F, Wang G (2009) Synthesis and UV shielding properties of zinc oxide ultrafine particles modified with silica and trimethyl siloxane. *Colloids Surf, A* 340:161–167
- De Castro SF, Da Silva MMF, Lima LCB, Osajima JA, da Silva Filho EC (2018) Modifying cellulose with metaphosphoric acid and its efficiency in removing brilliant green dye. *Int J Biol Macromol* 114:470–478

Table 3 Removal percentages and RSD% of BG and TBO dyes from different location of wastewater samples using TPUF@ZnO nanocomposite

Location	BG	TBO	Average%	RSD%
Nile water	92.5	99.7	97.3	4.23
Laundry water	78.7	82.1	79.8	2.52
Industrial wastewater	96.8	95.5	95.2	1.79



- El-Shahat MF, Moawed EA, Farag AB (2007) Chemical enrichment and separation of uranyl ions in aqueous media using novel polyurethane foam chemically grafted with different basic dyestuff sorbents. *Talanta* 71:236–241
- Hicham Z, Bencheqroun Z, El Mrabet I, Neves I (2019) Removal of basic dyes from aqueous solutions by adsorption onto Moroccan clay (Fez City). *Mediterr J Chem* 8:158–167
- Hou Y, Yan S, Huang G, Yang Q, Huang S, Cai J (2020) Fabrication of N-doped carbons from waste bamboo shoot shell with high removal efficiency of organic dyes from water. *Biores Technol* 303:122939
- Islam MdA, Ali I, Abdul Karim SM, Firoz MdSH, Chowdhury A, Morton DW, Angove MJ (2019) Removal of dye from polluted water using novel nano manganese oxide based materials. *J Water Process Eng* 32:100911
- Jiang X, Sun P, Xu L, Xue Y, Zhang H, Zhu W (2020) Platanus orientalis leaves based hierarchical porous carbon microspheres as high efficiency adsorbents for organic dyes removal. *Chin J Chem Eng* 28:254–265
- Kiwaan HA, Mostafa MR, El-Ghobashy H, Moawed EA (2020) Kinetic and equilibrium studies of the removal of crystal violet from aqueous solution using modified carbon. *J Sci Eng Res* 11:1022–1026
- Li JF, Rupa EJ, Hurh J, Huo Y, Chen L, Han Y, Jc A, Park JK, Lee HA, Mathiyalagan R, Yang D-C (2019) Cordyceps militaris fungus mediated zinc oxide nanoparticles for the photocatalytic degradation of Methylene blue dye. *Optics* 183:691–697
- Maleki A, Hamesadeghi U, Daraei H, Hayati B, Najafi F, McKay G, Rezaee R (2017) Amine functionalized multi-walled carbon nanotubes: single and binary systems for high capacity dye removal. *Chem Eng J* 313:826–835
- Moawed EA, El-Shahat MF (2006) Preparation, characterization and application of polyurethane foam functionalized with α -naphthol for preconcentration and determination of trace amounts of nickel and copper in cast iron and granite. *React Funct Polym* 66:720–727
- Moawed EA, El-Shahat MF (2013) Synthesis, characterization of low density polyhydroxy polyurethane foam and its application for separation and determination of gold in water and ores samples. *Anal Chim Acta* 788:200–207
- Moawed EA, El-Shahat MF (2016) Equilibrium, kinetic and thermodynamic studies of the removal of triphenyl methane dyes from wastewater using Iodopolyurethane powder. *J Taibah Univ Sci* 10:46–55
- Moawed EA, El-Hagrasy MA, Embaby NEM (2017) Substitution influence of halo polyurethane foam on the removal of bismuth, cobalt, iron and molybdenum ions from environmental samples. *J Taiwan Inst Chem Eng* 70:382–390
- Moawed EA, Wahba AE, Gabr RA (2018) Synthesis and application of LGB/St/Al₂O₃ biocomposite for sensitive detection and efficient removal of brilliant green dye from wastewater. *J Environ Chem Eng* 6:7225–7232
- Moawed EA, El-Hagrasy MA, Kamal M (2019a) Detection and removing of lead from wastewater using chemical treatment of polyurethane foam waste: batch and column experiments. *Desalin Water Treat* 159:338–345
- Moawed EA, Hegajy TA, Kosbar TR, Eissa MS (2019b) Removal of methylene blue dye from wastewater using ZnONPs in the dark and light. *Int J Sci Eng Res* 10:249–253
- Moawed EA, El-Hagrasy MA, Senan AEA (2019c) Application of bio alkyd resin for the removal of crystal violet and methylene blue dyes from wastewater. *Int J Environ Sci Technol* 16:8495–8504
- Mohamed MM, Ghanemb MA, Khairy M, Naguib E, Alotaibi NH (2019) Zinc oxide incorporated carbon nanotubes or graphene oxide nanohybrids for enhanced sonophotocatalytic degradation of methylene blue dye. *Appl Surf Sci* 487:539–549
- Mohanraj J, Durgalakshmi D, Balakumar S, Aruna P, Ganesan S, Rajendran S, Naushad Mu (2020) Low cost and quick time absorption of organic dye pollutants under ambient condition using partially exfoliated graphite. *J Water Process Eng* 34:101078
- Mostafa MH, Elsayy MA, Darwish MSA, Hussein LI, Abdaleem AH (2020) Microwave-Assisted preparation of Chitosan/ZnO nanocomposite and its application in dye removal. *Mater Chem Phys* 2481:122914
- Rauf MA, Qadri SM, Ashraf S, Al-Mansoori KM (2009) Adsorption studies of Toluidine Blue from aqueous solutions onto gypsum. *Chem Eng J* 150:90–95
- Shatnawi M, Alsmadi AM, Bsoul I, Salameh B, Mathai M, Alnawashi G, Alzoubi GM, Al-Dweri F, Bawa'aneh MS (2016) Influence of Mn doping on the magnetic and optical properties of ZnO nanocrystalline particles. *Results Phys* 6:1064–1071
- Stenholm A, Hedeland M, Arvidsson T, Pettersson CE (2020) Removal of nonylphenol polyethoxylates by adsorption on polyurethane foam and biodegradation using immobilized *Trametes versicolor*. *Sci Total Environ* 724:138159
- Tang Q, Wang K, Ren X, Zhang Q, Lei W, Jiang T, Shi D (2020) Preparation of porous antibacterial polyamide 6 (PA6) membrane with zinc oxide (ZnO) nanoparticles selectively localized at the pore walls via reactive extrusion. *Sci Total Environ* 715:137018
- Xu L, Zhang H, Tian Y, Jiao A, Chen F, Chen M (2019) Photochemical synthesis of ZnO@Au nanorods as an advanced reusable SERS substrate for ultrasensitive detection of light-resistant organic pollutant in wastewater. *Talanta* 194:680–688
- Yilmaz E, Salem S, Sarp G, Aydin S, Sahin K, Korkmaz I, Yuvali D (2020) TiO₂ nanoparticles and C-Nanofibers modified magnetic Fe₃O₄ nanospheres (TiO₂@Fe₃O₄@C-NF): a multifunctional hybrid material for magnetic solid phase extraction of ibuprofen and photocatalytic degradation of drug molecules and azo dye. *Talanta* 2131:120813
- Zhang Y, Yang L, Wang Y-H, Liu A-H (2019) MoxPy nanoparticles supported on mesh structural carbon from biomass for rapid selective dyes adsorption. *Talanta* 196:1–17

